ROYAL SOCIETY
OF CHEMISTRY

PAPER

Quinoidal thioalkyl-substituted bithiophene small molecule semiconductors for n-type organic field effect transistors†

Vellaichamy Joseph, [iD] ‡[a] Chih-Hsin Yu,‡[b] Chia-Chi Lin,‡[b] Wei-Chieh Lien,[a] Hsin-Chia Tsai,[a] Cheng-Shiun Chen,[a] Alfonsina Abat Amelenan Torimtubun, [iD] [b] Arulmozhi Velusamy,[a] Ping-Yu Huang,[a] Gene-Hsiang Lee,[c] Shueh-Lin Yau,[a] Shih-Hung Tung, [iD] [d] Takeo Minari, [iD] [e] Cheng-Liang Liu [iD] *[f] and Ming-Chou Chen [iD] *[a]

Two tetrathioalkyl-substituted bithiophene-based small molecule quinoids (**TSBTQ**s) having different chain lengths (thio-hexyl and -decyl) are synthesized and applied as an n-type active component in organic field effect transistors (OFETs). The resulting two **TSBTQ**s exhibit good solubility in various organic solvents and LUMO levels below −4.0 eV. The theoretical DFT calculation supported by single crystal structures confirms the π-conjugated backbone planarity due to the S(thiophene)···S(alkyl) non-covalent interaction. Optimized **TSBQT-10** OFETs exhibit an electron mobility of 0.18 cm^2 V^{-1} s^{-1}, which is higher than that of **TSBTQ-6** (0.09 cm^2 V^{-1} s^{-1}). The reliability of the OFETs under representative environmental and operational conditions is also determined. The effects of side chains including their lengths and contribution to the main chain π-system coplanarity presented here demonstrate an efficient method to manipulate the charge carrier mobility of the quinoidal organic semiconductors.

Introduction

Organic π conjugated materials have emerged as the backbones of low-cost electronic devices that will appear on the market in the near future.[1–3] In particular, organic small molecules possessing precise properties are superior to their polymeric counterparts due to their well-defined structure, easy purification and facile functional modification.[4–7] The charge carrier mobility of organic materials determines their prospective applications in optoelectronic devices, in particular organic field-effect transistors (OFETs). Accordingly, many studies reported the design of

conjugated materials and their application in optimized device architectures to realize high carrier mobility.[8–14] Organic materials that find applications in OFETs can be classified as p-type and n-type materials. So far, p-type semiconducting materials have achieved significant milestones in charge mobility and device stability, while n-type materials are still lagging behind owing to their low mobility. Thus, the development of n-type materials exhibiting high mobility is needed.[15–27] To date, there have been different classes of conjugated materials that show n-type semiconducting properties in the literature. For example, tetra-azapentacenes,[28–30] diketopyrrolopyrrole (DPP)[31,32] naphthalene-diimide (NDI),[33–35] perylenecarboxydiimide (PDI)[36] and oligo-/fused thiophenes[23–27] with encapsulated electron withdrawing groups, such as perfluorophenyls,[37–39] cyano,[40] and alkyl cyanoacetates,[9] are all notable materials (Fig. 1 and 2).

In particular, Professors Tobin Marks and Antonio Facchetti were the first pioneers that developed oligothiophenes end capped with the fluoroalkyl/perfluorophenyl group as n-type semiconductors. They fabricated the **DFHCO-4T** based OFET device and optimized it to get an excellent electron mobility of up to 2.0 cm^2 V^{-1} s^{-1} (Fig. 1A–C).[23–25] Later, Marks, Facchetti, and Chen explored fused oligothiophenes end capped with perfluorophenyl as n-type materials for OFETs and an electron mobility of up to 0.3–0.43 cm^2 V^{-1} s^{-1} was achieved (Fig. 2H–J).[26,38,39]

Among the various newly developed n-type materials, quinoidal thiophenes are getting much attention owing to their inherent

[a] *Department of Chemistry and Research Center of New Generation Light Driven Photovoltaic Module, National Central University, Taoyuan 32001, Taiwan. E-mail: mcchen@ncu.edu.tw*

[b] *Department of Chemical and Materials Engineering, National Central University, Taoyuan 32001, Taiwan*

[c] *Instrument Center, National Taiwan University, Taipei 10617, Taiwan*

[d] *Institute of Polymer Science and Engineering, National Taiwan University, Taipei 10617, Taiwan*

[e] *Research Center for Functional Materials, National Institute for Materials Science, 1-1 Namiki, Tsukuba, Ibaraki 305-0044, Japan*

[f] *Department of Materials Science and Engineering, National Taiwan University, Taipei, 10617, Taiwan. E-mail: liucl@ntu.edu.tw*
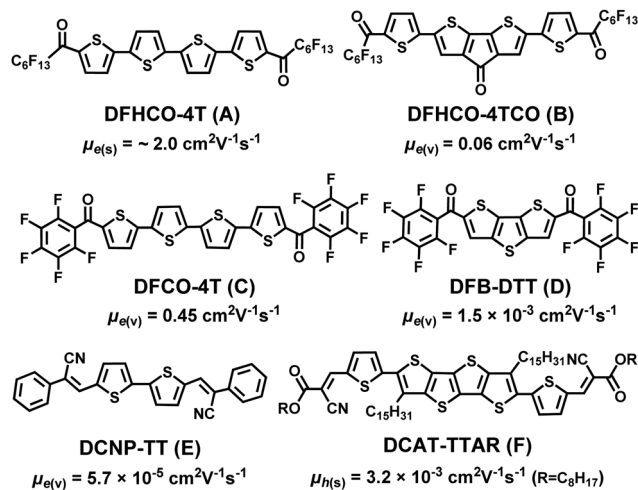
‡ These authors contributed equally to this work.

Fig. 1 Examples of n-type oligo/fused thiophenes endcapped with fluoro-alkyl/phenyl, cyano and alkyl cyanoacetates. Symbols (μ_e) and (μ_h) denote electron and hole mobility, respectively, while (v) and (s) denote semiconductor films obtained from vacuum and solution processes, respectively.
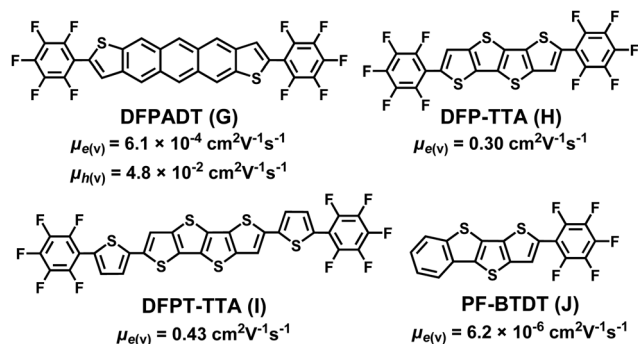

Fig. 2 Examples of n-type fused oligothiophenes flanked by perfluorophenyls. The symbols (μ_e) and (μ_h) denote electron and hole mobility, respectively, while (v) denotes semiconductor films obtained from the vacuum process.

planar molecular structure and tendency to crystallize in a face-to-face manner that eventually facilitates charge mobility in the thin film state.[40–42] Furthermore, quinoidal compounds possess special characteristics of superior π orbital overlapping over the aromatic structure. This structural feature enables effective π electronic conjugation across the molecular backbone and thus improves planarity. The rigidity enabled planar structure contributes to facile charge transport through restricted conformational disorder. Furthermore, the quinoidal structure stabilizes electronic defects such as biradicals and thereby strengthens/retains the conjugated system.[44–46] The incorporation of alkyl chains and modification of chain length on oligothiophenes enable a good solution-processing ability and favor electron mobility as a result of different molecular ordering in the solid state.[47–49] Interestingly, thioalkylated/alkoxy-lated π conjugated scaffolds are superior to their conventional alkylated counterparts and provide highly efficient solution processable OFETs. The weak intramolecular interaction between S···S/ S···O contacts may prevent repulsion between the alkyl chain and arene core. On the other hand, these interactions make the core

more rigid and eventually induce molecular crystallinity. Furthermore, the sulfur atom present in the thioalkyl chain provides an intramolecular lock with the sulfur atom of the neighboring thiophene unit and thus enhances molecular planarity and carrier mobility.[50–54] Generally, the double-bond character of both quinoidal termini is retained by the use of end-cappers.

Dicyanomethylene encapsulation is used to afford n-type semiconducting behavior.[55–57] Thus, the electron withdrawing dicyanomethylene end-capped materials have been examined with the aim to achieve both n-type semiconducting behavior as well as to retain the double-bond character in quinoidal compounds (Fig. 3).[5,43,58–63] Since the electrical properties of organic materials are highly dependent on their chemical structure, the design and synthesis of organic semiconducting materials and their correlation with regard to the structure–function relationship are of great interest.

In this report, we have designed and synthesized bithiophene-based quinoidal compounds (**TSBTQ**s) containing tetrathioalkyl groups with different alkyl chain lengths on thiophene to modulate the solubility and molecular stacking in the thin film state that could help optimize electron mobility in the device. The combination of S···S (thioalkyl group and thiophene core) interaction and a suitable alkyl chain ($C_{10}H_{21}$) in **TSBTQ**s paved the way for the effective molecular planarity and solution processability of quinoidal **TSBTQ** structures. Moreover, the encapsulation of the electron withdrawing dicyano group on this core resulted in the n-type semiconducting property for these molecules. As a result, the OFET device based on **TSBTQ-10**
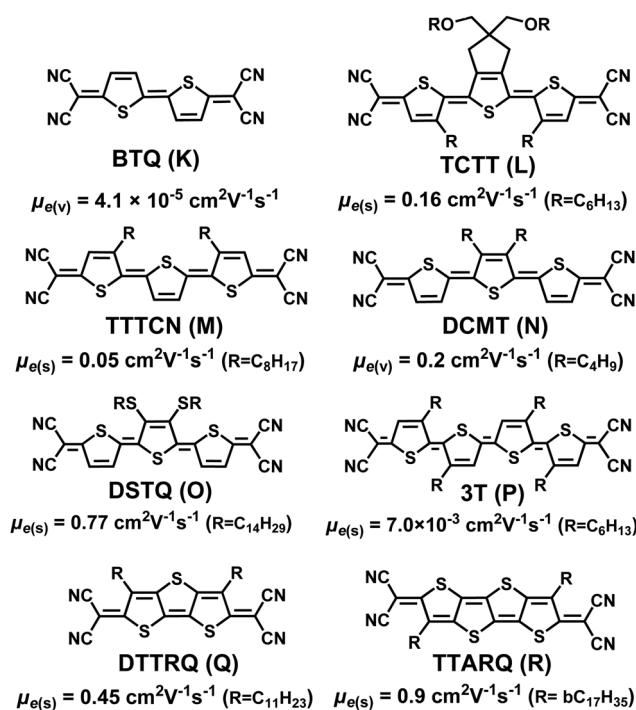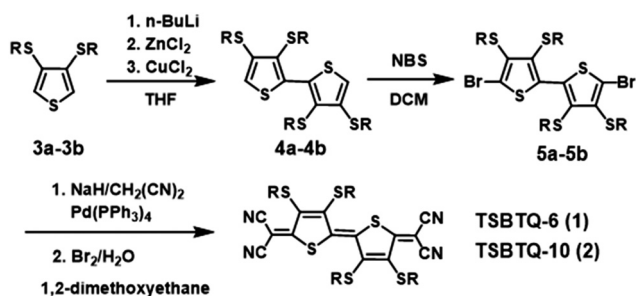

Fig. 3 Examples of n-type small molecule quinoidal oligo/fused thiophenes. The symbol (μ_e) denotes electron mobility, while (v) and (s) denote semiconductor films obtained from vacuum and solution processes, respectively.

showed the highest electron mobility of 0.18 cm^2 V^{-1} s^{-1}. For comparison, vacuum deposited quinoidal bithiophene **BTQ** (Fig. 3) showed the lowest mobility due to there being less π–π interaction[58] while quinoidal terthiophene **DCMT** (Fig. 3) gave a mobility of 0.2 cm^2 V^{-1} s^{-1} under high vacuum.[59] In contrast, our **TSBTQ** compounds are solution processable thanks to the long alkyl chains and thus exhibited comparable electron mobility. Furthermore, the new developed TSBTQs possess a low lying LUMO (<4.0 eV) relative to a vacuum that suppresses the air oxidation and thus achieves good ambient stability. In addition, the strong electron withdrawing dicyanomethylene groups provide short N···S intermolecular contact (*vide infra*), which prompts the formation of good molecular stacking and elicits good electron mobility.

Results and discussion

The synthetic pathway for the quinoids is depicted in Scheme 1. 3,4-Bis(alkylthio)thiophenes (**3a** and **3b**) were first lithiated to afford 3,3′,4,4′-tetrakis(alkylthio)-2,2′-bithiophenes (**4a** and **4b**). Bromination of the latter resulted in 5,5′-dibromo-3,3′,4,4′-tetrakis(alkythio)-2,2′-bithiophenes (**5a** and **5b**). The dibrominated bithiophenes (**5a** and **5b**) were then converted into the respective quinoidal compounds (**1** and **2**) by the palladium-catalyzed Takahashi coupling reaction and subsequent oxidation using bromine/water. The quinoidal compounds (**TSBTQ-6** and **TSBTQ-10**) were obtained in the form of blue-black powders with the yields of 59 and 65%, respectively. These two target compounds were found to be highly soluble in common organic solvents, such as tetrahydrofuran, chloroform, and chlorobenzene, which makes them convenient in the fabrication of solution-processable organic semiconductor thin films for transistor devices. Such good solubility is presumably due to the four long thioalkyl solubilizing side chains attached on the bithiophene core. All the chemical structures of **TSBTQ** compounds and intermediates were characterized by ^{1}H/^{13}C NMR spectroscopy and mass spectrometry, and the obtained data were found to be consistent with the proposed structure.

The thermal properties of the newly synthesized **TSBTQ** compounds were studied by differential scanning calorimetry (DSC) and thermogravimetric analysis (TGA) recorded under a nitrogen atmosphere. The corresponding thermal data are compiled in Table 1. Both samples showed sharp endothermic peaks

Table 1 Thermal, optical and electrochemical properties of the compounds

Compound	$T_m{}^a$ [°C]	$T_d{}^b$ [°C]	$\lambda_{max}{}^c$ [nm]	$E_g{}^d$ [eV]	$E_{ox}{}^e$ [V]	$E_{red}{}^e$ [V]	HOMO [eV]	LUMO [eV]
TSBTQ-6	139	242	625	1.62	1.78	0.16	−5.98	−4.36
TSBTQ-10	107	242	625	1.62	1.78	0.16	−5.98	−4.36

^{a} By DSC. ^{b} By TGA. ^{c} In THF. ^{d} Calculated from the film absorption edge. ^{e} By DPV in o-C$_6$H$_4$Cl$_2$. HOMO = −(4.2 + E_{ox}); LUMO = −(4.2 + E_{red}).

with melting points (T_m) above 100 °C (Fig. S1 of the ESI†). The thermal decomposition temperatures (T_d, 5% weight loss) were determined by TGA analysis (Fig. S2 of the ESI†), which were greater than 240 °C, and this is attributed to the rigidity of the dicyanomethylene encapsulated bithiophene quinoidal structure.[64] The thermal degradation of these compounds arises from the cleavage of labile alkyl chains, which is attested by the TGA weight loss profile.

The absorption properties of the **TSBTQ** compounds were studied in diluted solution and thin films (Fig. 4 and Fig. S21, ESI†), and the detailed optical parameters are shown in Table 1. Both the compounds exhibited similar spectral features (400–700 nm) with an identical absorption maximum of 625 nm. The broad peak is extended up to 700 nm, which stems from the π–π* transition of the entire molecular backbone,[65,66] indicating that the side chain length does not influence the π-conjugation. The maximum of the absorption spectra of **TSBTQ-6** and **TSBTQ-10** in films exhibited a red-shift of 113 nm relative to that in solution, which is mainly due to molecular aggregation from strong intermolecular interaction. Besides, the optical band gaps of **TSBTQ-6** and **TSBTQ-10** calculated from the absorption onset edges of the thin film absorption are 1.63 and 1.62 eV, respectively, which provide good semiconducting characteristics.

The electrochemical properties of the compounds were investigated by differential pulse voltammetry (DPV) recorded in o-dichlorobenzene using 0.1 M Bu$_4$NPF$_6$ as a supporting

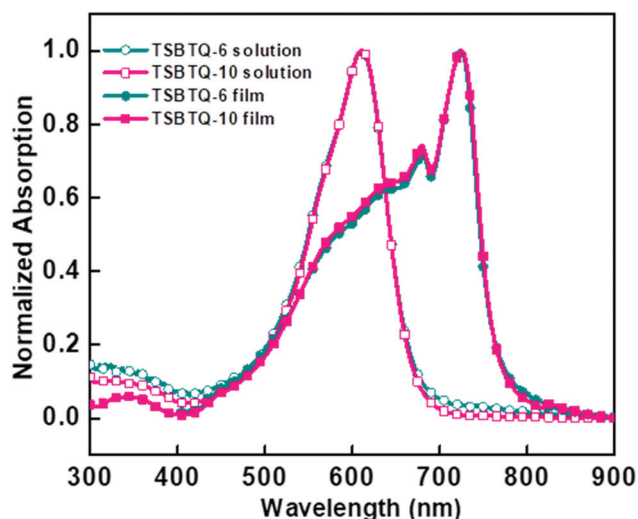**Scheme 1** Synthetic protocol for **TSBTQ** compounds.

Fig. 4 UV-Vis absorption spectra of **TSBTQ** compounds recorded in diluted solution (hollow dotted line) and solution-sheared films (solid dotted line).
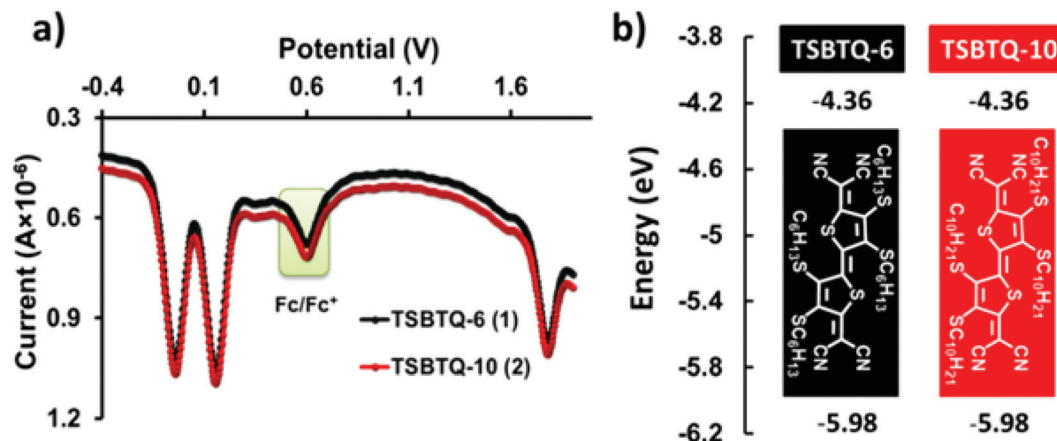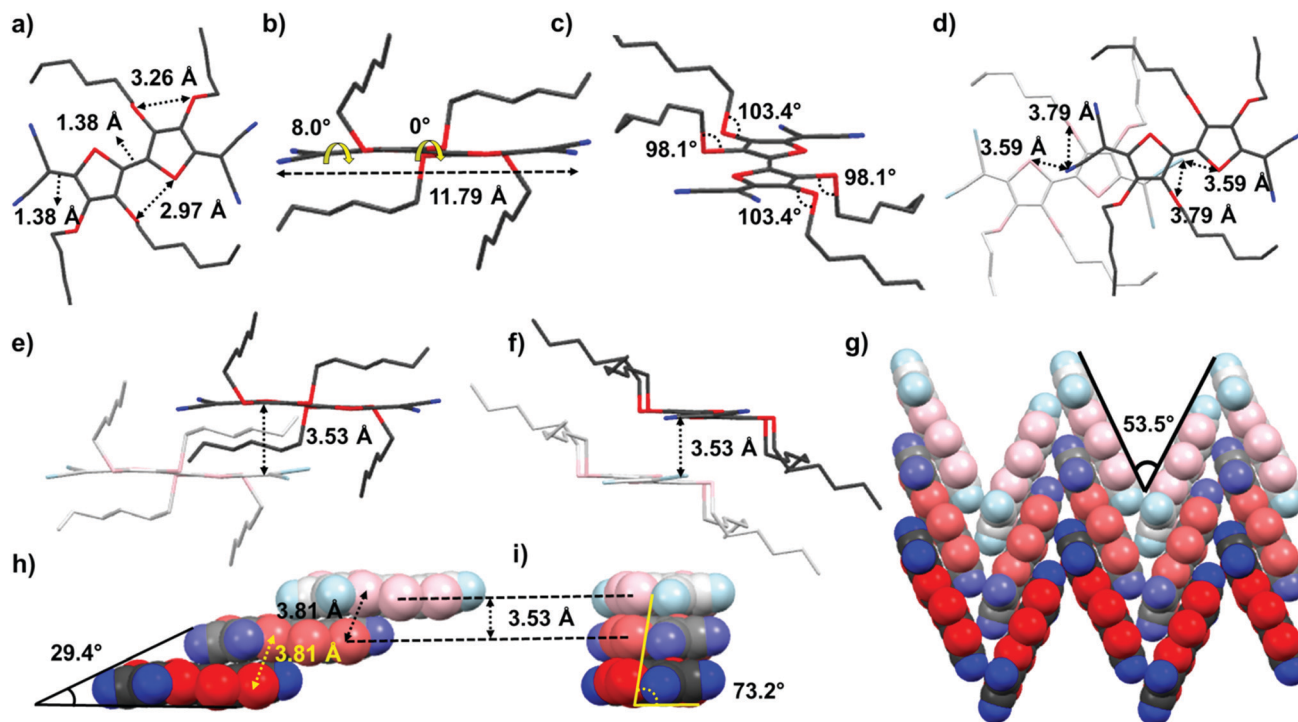
15452 | *J. Mater. Chem. C*, 2020, **8**, 15450–15458

This journal is © The Royal Society of Chemistry 2020

Fig. 5 (a) DPV of **TSBTQ**s recorded in *o*-dichlorobenzene. (b) DPV-derived HOMO and LUMO energy levels.

electrolyte to determine the HOMO and LUMO energy levels. The observed differential pulse voltammograms of all the compounds are presented in Fig. 5a, and the relevant oxidation/reduction potentials are noted in Table 1. The oxidation/reduction potential of these two **TSBTQ**s was estimated to be 1.78/0.16 V, corresponding to the HOMO/LUMO energy level of $-5.98/-4.36$ eV (energy diagram in Fig. 5b). The electrochemical potential of the derivatives is invariant with respect to changes in alkyl chain substitution.[67] The low-lying LUMO of these quinoidal compounds (< -4.2 eV) affirms their potential for ambient stability and good electron mobility for OFET applications.[68,69] Furthermore, the LUMO of the compounds almost matches the work function of the silver electrode (-4.26 eV), which ensures facile electron injection.

The ground state geometry and frontier molecular orbitals were computed with density functional theory (DFT) at the B3LYP/6-31G* level (Fig. S3 of the ESI†). The theoretical calculation reveals that the S–C–C–S dihedral angle between the two central thiophene cores (linkage adopts an anti-conformation) in **TSBTQ**s is almost zero. This near-coplanar configuration along the molecular axis may be due to the strong intramolecular S(thiophene)···S(alkyl) interaction or quinoidal form in the bithiophene moieties. From the theoretical distributions of the frontier molecular orbitals, both the HOMO and LUMO of these two compounds delocalize throughout the entire molecule due to the planarized thioalkyl-substituted bithiophene. The energy levels of the HOMO and LUMO were estimated to be -6.15 and -4.23 eV, respectively, indicating that the **TSBTQ**s are predominately n-type small molecule semiconductors. The differences between the experimentally and theoretically estimated energy levels are attributable to the aggregated state/gas phase and the approximations made.

In order to gain deep insight into the molecular stacking pattern and its implications for the charge transport properties, a single crystal XRD pattern of **TSBTQ-6** was obtained. The single crystal of **TSBTQ-6** was grown by a slow solvent evaporation method. The molecular structure and the complete crystal data derived from X-ray crystallographic analysis are shown in Fig. 6 and Fig. S4 (ESI†). As shown in Fig. 6, **TSBTQ-6** (**1**) crystallizes in the monoclinic space group of *C*2/*c* (Table S1,

ESI†). The intramolecular distances of S(thiophene)···S(alkyl) of neighbouring thiophenes and S(alkyl)···S(alkyl) in the same thiophene unit are 2.97 and 3.26 Å, respectively, which are less than the sum of the van der Waals radius of the S atom (3.70 Å). Both CN-capped methylene end groups to the TSBT core have a C–C distance of 1.38 Å, exhibiting double bond characteristics (Fig. 6a). The **TSBTQ** main core and the two end-capped CN groups are nearly coplanar, with a small torsion angle of 8.0° and its molecular length is 11.79 Å. The TSBT core is highly planar, as confirmed from the torsion angle of 0° and a central C–C distance of 1.38 Å (characteristic of a double bond) between two thiophene units (Fig. 6b). The four thio-hexyl chains are well-aligned (two in the upward direction and the other two in the downward direction to the core) to form good planar stacking layers of **TSBTQ**. Thus, two thio-hexyl chains on each side show bending angles of 103.4° and 98.1° out of the **TSBTQ** core (Fig. 6c). It should be noted that four thio-alkyl chains distort on the TSBT core in the same direction, which enables a good stacking arrangement (Fig. S4 of ESI†). The TSBT cores are connected by the closely adjacent S···N contacts with the intermolecular S···N distances of 3.59 and 3.79 Å (Fig. 6d). Front and side view stacking **TSBTQ-6** molecules show a π–π stacking distance of 3.53 Å (Fig. 6e and f). The **TSBTQ** molecules are linked in "zig-zag" connection layers and the layers exhibit a "herringbone packing" arrangement. In each layer, the "zig-zag" angle between two neighbouring **TSBTQ** cores is 53.5° (Fig. 6g). Among each layered stack, the **TSBTQ** cores are spaced at a distance of 3.53 Å and possess an interlayer S···S distance of 3.81 Å with layer-slipping angles of 29.4° and 73.2° (Fig. 6h and i). In summary, the planar molecular structure, short intermolecular stacking distance (3.53 Å), short inter and intramolecular S···S and S···N distances, and main arrangement of thio-alkyl chains toward the core suggest that **TSBTQ-6** possesses ideal characteristics for extended π-orbital interaction, resulting in decent device performance (*vide infra*). The charge transport in this packing structure can be achieved either through herringbone stacked molecules, or through the well "zig-zag" connected neighbouring molecules. The **TSBTQ-6** quinoidal structure is quite planar

This journal is © The Royal Society of Chemistry 2020

J. Mater. Chem. C, 2020, **8**, 15450–15458 | **15453**

Fig. 6 Single crystal structure of **TSBTQ-6** in stick models (a–f) and space filling packing models (g–i). (a) Top view of **TSBTQ-6** with intramolecular S···S and C–C distances. (b) Front view of **TSBTQ-6** with a molecular length of 11.79 Å. The end-capping CN group planes to the **TSBTQ** central plane with a small dihedral angle of 8.0°. The TSBT core is highly planar with a torsion angle of 0°. (c) Side view of **TSBTQ-6** with >98° bending angles of two thio-hexyl chains to the planar core. (d–f) Stacking molecules of **TSBTQ-6** with a π–π stacking distance of 3.53 Å and the intermolecular S···N distances are 3.59 and 3.79 Å. (g–i) Molecular packing arrangement of **TSBTQ-6** with a herringbone stacking distance of 3.53 Å exhibiting slipping angles of 29.4° and 73.2°. The zig-zag angle between two neighbouring **TSBTQ** cores is 53.5°. In the **TSBTQ** stacking, the interlayer S···S distance is 3.81 Å. The red (light red), blue (light blue) and gray (and light gray) colored balls indicate sulphur, nitrogen, and carbon atoms, respectively.

with a small distortional angle that may be beneficial for good charge carrier transport.

The OFET devices use a bottom-gate top-contact (BGTC) structure with solution-shearing as the film deposition method. The OFET characteristics were evaluated using **TSBTQ**s as the active channel onto the silanized Si/SiO$_2$ substrate. Detailed procedures of device fabrication and measurement are described in the Experimental section. Solution-shearing is one of the single-step meniscus-guided coating methods that can produce crystalline thin films. The **TSBTQ**-based OFETs exhibited predominant n-type behavior due to the low energetic barrier between the LUMO and Fermi level of the silver contacts, and the electron mobilities can be obtained from the saturation region of the transfer curves. Fig. 7 and Fig. S5 of the ESI† show the transfer (drain-to-source current (I_{ds}) *vs.* gate voltage (V_g)) and output (drain-to-source current (I_{ds}) *vs.* drain-to-source voltage (V_{ds})) curves and Table 2 summarizes the detailed OFET performance data. The solution-sheared **TSBTQ-6** and **TSBTQ-10** exhibited maximum/average electron mobilities (μ_{max}/μ_{avg}) of 0.09/0.04 ± 0.02 and 0.18/0.13 ± 0.03 cm^2 V^{-1} s^{-1}, an ON/OFF ratio (I_{ON}/I_{OFF}) of 10^3–10^4 and 10^4–10^5, and a threshold voltage (V_{th}) of 13.6 ± 6.7 and 24.5 ± 6.2 V, respectively. A slightly higher mobility of the **TSBTQ-10** device with a greater side chain length can be obtained, probably due to the optimized microstructures with a higher crystallinity. This can be further proved by the AFM and GIXRD analyses.
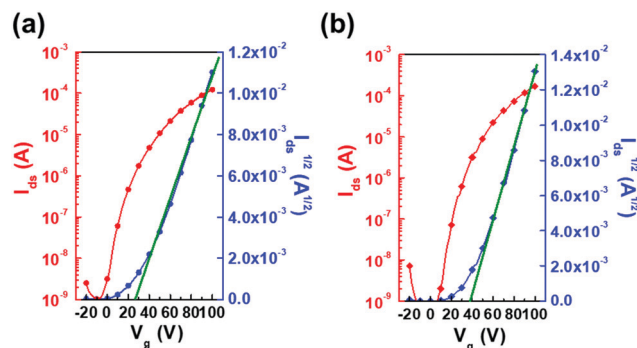
Fig. 7 Representative transfer characteristics of solution-sheared OFETs based on (a) **TSBTQ-6** and (b) **TSBTQ-10** compound thin films.

In addition, these solution-sheared films are quite thick and rough; thus in a top-contact OFET architecture, this means that there is quite a large depletion region that the injected charge has to penetrate before approaching the channel. This also contributes to the large V_{th}. Additional contribution to V_{th} may arise from the large crystalline grains separated by large grain boundaries. A consequence of the relatively thick semiconducting films in combination with OFET processing in an ambient rather than N$_2$-filled glove box may induce possible sources of traps in the films or between the interlayer. The threshold voltage could

15454 | *J. Mater. Chem. C*, 2020, **8**, 15450–15458

This journal is © The Royal Society of Chemistry 2020

Table 2 Summary of OFET parameters based on **TSBTQ-6** and **TSBTQ-10**

Sample	μ_{max} (cm^2 V^{-1} s^{-1})	μ_{avg} (cm^2 V^{-1} s^{-1})	I_{ON}/I_{OFF} (—)	V_{th} (V)
TSBTQ-6	0.09	0.04 ± 0.02	10^3–10^4	24.5 ± 6.2
TSBTQ-10	0.18	0.13 ± 0.03	10^4–10^5	35.2 ± 7.9

be further reduced if all the processing procedures were done in a low H_2O/O_2 atmosphere and a high dielectric constant/reduced thickness of the dielectric layer can be applied.[70,71] Furthermore, the mobilities of **TSBTQ-6** achieved by spin-coating (transfer curve in Fig. S6 of the ESI†) are much lower than those achieved by solution-shearing (~100-fold), which was also confirmed by our previous report.[5,43,53] All the results suggested that using the solution-shearing technique for thin film deposition can enhance crystallinity and promote molecular orientation, thus enhancing charge transport.[5,43,53]

Morphological analysis of the active layer of the organic semiconductors was performed to understand the effects of molecular organization using POM and AFM. Fig. 8 shows the POM and AFM images of the **TSBTQ**s assembled at a fixed shearing speed with a fixed solution concentration similar to the optimized OFET device. The film exhibits strip patterns with a millimeter-sized extension. AFM images also indicate aligned crystalline arrays with a width of dozens of micrometers. However, the rougher **TSBTQ-10** surfaces as compared to **TSBTQ-6** (root-mean-square roughness (R_{rms}): 14.2 and 6.8 nm, respectively)
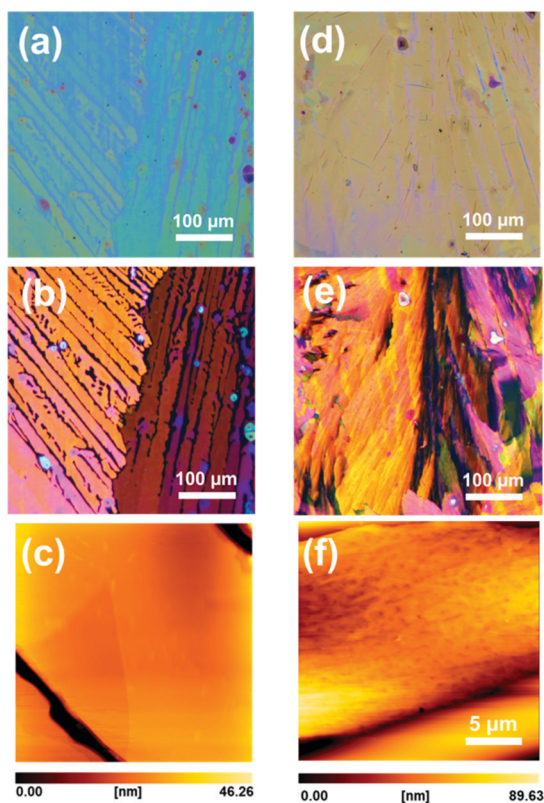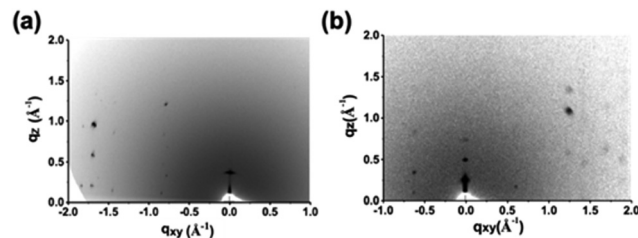

Fig. 9 2D GIXRD patterns of solution-sheared (a) **TSBTQ-6** and (b) **TSBTQ-10** thin films.

suggest that a larger crystalline grain with reduced grain boundaries may be formed.

2D GIXRD analysis was conducted to clarify the crystallinity and molecular packing orientation of the **TSBTQ** film (Fig. 9). Fig. S7 of the ESI† shows the 1D diffraction pattern with respect to the out-of-plane (OOP) and in-plane (IP) directions, as extracted from 2D GIXRD results. Both **TSBTQ** films show edge-on structures with lamellar stacking along the q_z direction. The d-spacing of **TSBTQ-6** lamellar stacking is 17.4 Å, which is close to half the a length of the unit cell (36.5 Å in Table S1, ESI†). The π–π spacing of **TSBTQ-6** calculated from the diffraction spot at q_{xy} = 1.75 Å^{-1} is 3.59 Å, close to a single crystal π–π stacking distance of 3.53 Å, as shown in Fig. 6h. Both the d-spacings confirm that the crystal structure of **TSBTQ-6** formed under shearing is similar to that of the single crystal. The lamellar d-spacing of **TSBTQ-10** is 25.4 Å, higher than that of **TSBTQ-6** due to the longer side chain. In particular, the strong and higher-order Bragg diffraction texture along the q_z direction in **TSBTQ-10** represents a highly crystalline and ordered film as compared to **TSBTQ-6**. The longer side chain on **TSBTQ-10** may improve the coplanarity of the bithiophene quinoids and increase the solubility of **TSBTQ-10** in the solvent, both of which may contribute to the highly ordered structure obtained using the solution-shearing process.

A comparison of the environmental stability of **TSBTQ-6** and **TSBTQ-10** upon exposure to environmental conditions (relative humidity (RH) of 20–30% and room temperature) was conducted. Fig. 10a shows the normalized temporal changes of I_{ds} measured on champion devices in the saturation region ($V_g = V_{ds}$ = 100 V) for 35 days. It is clear that the I_{ds} does not obviously degrade during prolonged exposure. Both **TSBTQ-6** and **TSBTQ-10** maintained an

Fig. 8 (a and d) OM, (b and e) POM and (c and f) AFM images of solution-sheared **TSBTQ-6** and **TSBTQ-10** compound thin films.
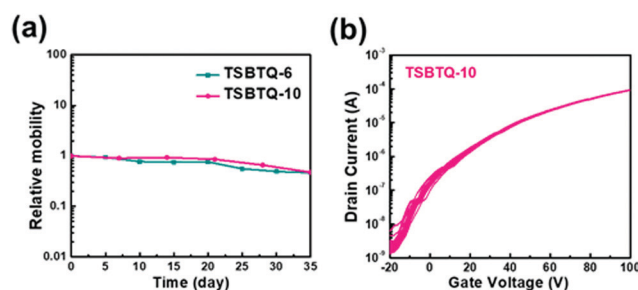

Fig. 10 (a) Long-term ambient stability of **TSBTQ** OFETs based on Ag source and drain contacts, stored at 20–30% humidity. (b) The operation stability of **TSBTQ** OFETs.

This journal is © The Royal Society of Chemistry 2020

J. Mater. Chem. C, 2020, 8, 15450–15458 | 15455

OFET response under ambient conditions, regardless of the difference in the microstructural film morphologies. These results indicate that the observed stability mainly originates from the low-lying LUMO energy level (less than -4.0 eV) of **TSBTQ** materials, which can stabilize the radical anion forms of the organic semiconductor toward H_2O and/or O_2.[72,73] Both **TSBTQ** samples form edge-on structures with out-of-plane (q_z) (001) layer distances of 17.4 and 25.4 nm for **TSBTQ-6** and **TSBTQ-10** films, respectively, and these distance can be related to the lamellar distances between the two main conjugated backbones determined by the length of the lateral side chain. Fig. 10b and Fig. S8 of the ESI† illustrate the operation stability of the **TSBTQ** OFETs. The transfer characteristics of the devices were measured by continuously sweeping V_g from -20 to 100 V at $V_d = 100$ V in a nitrogen-filled glove box. All the transfer curves almost overlap over 100 scans, and no detectable ON current or ON/OFF ratio degradation or shift in V_{th} can be observed, indicating that the **TSBTQ** films with minimized grain boundaries exhibit better electrical stability.[74]

Conclusions

In conclusion, two solution-processable dicyanomethylene end-capped bithiophene quinoids with four inserted thioalkyl side chains have been synthesized to study the effects of side chain length on the electron mobility of OFET devices. In the DFT calculation and single crystal XRD, **TSBTQ** exhibited good backbone planarity in the central bithiophene core due to the non-covalent interactions between the sulfur atom in thiophene (S-thienyl) and the sulfur atom in the neighboring thioalkyl chain (S-thioalkyl). Despite similar frontier energy levels, **TSBTQ-10** exhibits a relatively higher mobility of >0.1 cm^2 V^{-1} s^{-1} due to morphological factors, such as the highly crystalline and ordered structures with a shorter π–π distance. Furthermore, the device performance and in particular the excellent environmental and operational stability can be reproduced. We believe that our findings can encourage others to design building blocks in a quinoidal π-system that can be used to develop high performance solution-processable small molecule OFETs.

Experimental section

Materials synthesis

Malononitrile (1.2 mmol) was added to a round bottom flask containing sodium hydride (2.4 mmol) in dry dimethoxyethane (30 mL) at 0 °C. The mixture was warmed to room temperature and stirred for 20 min. Bromo compounds (**5a–5b**; 0.3 mmol) and tetrakis(triphenylphosphine)palladium (0.09 mmol) were added to the mixture sequentially. This reaction mixture was refluxed for 6 h under a nitrogen atmosphere. Then, it was cooled to room temperature and the reaction was quenched by adding saturated bromine water at 0 °C and stirred for 15 min. The mixture was extracted with CH_2Cl_2, washed with brine solution and dried over Na_2SO_4. The organic layer was evaporated to yield

a residue, which was then purified by column chromatography using CH_2Cl_2/hexanes (1 : 5).

Synthesis of TSBTQ-6 (1). The title compound was obtained as a dark purple solid. Yield 117 mg (59%). M.p. 138 °C. ^{1}H NMR (500 MHz, CDCl$_3$) δ 3.03 (t, J = 6.8 Hz, 8 H), 1.70–1.62 (m, 8 H), 1.42–1.29 (m, 24 H), 0.88 (t, J = 5.6 Hz, 12 H). ^{13}C NMR (125 MHz, CDCl$_3$): δ 168.75, 156.17, 149.07, 138.67, 114.08, 112.65, 71.31, 39.39, 38.14, 31.23, 30.90, 29.71, 29.44, 28.43, 28.32, 22.48, 22.44, 13.97. HRMS (m/z FAB+) calcd for $C_{38}H_{52}N_4S_6$: 756.2516. Found: 756.2523.

Synthesis of TSBTQ-10 (2). The title compound was obtained as a dark purple compound. Yield (126 mg) 65%. M.p. 109 °C. ^{1}H NMR (500 MHz, CDCl$_3$) δ 3.02 (m, 8 H), 1.71–1.62 (m, 12 H), 1.61–1.26 (m, 8 H), 1.41–1.26 (m, 52 H), 0.88 (t, J = 5.5 Hz, 12 H). ^{13}C NMR (125 MHz, CDCl$_3$): δ 168.74, 156.16, 149.09, 138.67, 114.08, 112.65, 71.31, 39.38, 38.14, 31.88, 29.75, 29.52, 29.48, 29.29, 29.08, 28.78, 28.66, 22.67, 14.10. HRMS (m/z FAB+ (M + 1)) calcd for $C_{54}H_{84}N_4S_6$:981.5099. Found: 981.5090.

Device fabrication and measurement

Heavily n-doped Si/SiO$_2$ (300 nm) was used as the substrate for the OFETs in this study. The substrates were cleaned in an ultrasonic bath with acetone and isopropanol for 10 min each. Subsequently, the substrates were dried under a nitrogen flow, surface-treated with plasma for 5 min and then silanized by PETS. Then, 3–5 mg mL^{-1} solutions of **TSBTQ**s in 1,2-dichloro-benzene were solution-sheared onto the substrate at a shearing speed of 10–60 μm s^{-1} and a deposition temperature of 70–80 °C. The shearing apparatus setup is similar to that in our previous report.[5,43] The samples were thermally annealed at 80 °C overnight under vacuum. Finally, 80 nm-thick Au source/drain electrodes were thermally evaporated onto the organic semiconductor films through a shadow mask under a pressure of 10^{-6} Torr. The length (L) and width (W) of the channel were 25 and 1500 μm, respectively. The OFETs without specific encapsulation were tested on a probe station connected to a Keithley 4200-SCS semiconductor parameter analyzer in a N$_2$-filled glove box. The mobility was extracted from the square root of the transfer curve in the saturation region using the following equation:

$$\mu = \frac{2L}{WC}\left(\frac{\partial \sqrt{I_d}}{\partial V_g}\right)^2$$

where I_d is the drain current, V_g is the gate voltage, and C is the capacitance per unit area of the gate insulator.

Conflicts of interest

There are no conflicts to declare.

Acknowledgements

15456 | *J. Mater. Chem. C*, 2020, **8**, 15450–15458

This journal is © The Royal Society of Chemistry 2020

Notes and references

1 Y. Shirota, *J. Mater. Chem.*, 2000, **10**, 1–25.

2 K. Yamamoto, Y. Ie, M. Nitani, N. Tohnai, F. Kakiuchi, K. Zhang, W. Pisula, K. Asadi, P. W. M. Blom and Y. Aso, *J. Mater. Chem. C*, 2018, **6**, 7493–7500.

3 P. Andersson Ersman, R. Lassnig, J. Strandberg, D. Tu, V. Keshmiri, R. Forchheimer, S. Fabiano, G. Gustafsson and M. Berggren, *Nat. Commun.*, 2019, **10**, 5053.

4 H. Wang, J. Huang, M. A. Uddin, B. Liu, P. Chen, S. Shi, Y. Tang, G. Xing, S. Zhang, H. Y. Woo, H. Guo and X. Guo, *ACS Appl. Mater. Interfaces*, 2019, **11**, 10089–10098.

5 S. Vegiraju, G.-Y. He, C. Kim, P. Priyanka, Y.-J. Chiu, C.-W. Liu, C.-Y. Huang, J.-S. Ni, Y.-W. Wu, Z. Chen, G.-H. Lee, S.-H. Tung, C.-L. Liu, M.-C. Chen and A. Facchetti, *Adv. Funct. Mater.*, 2017, **27**, 1606761.

6 D. Ho, S. Vegiraju, D. Choi, C.-H. Cho, G. Kwon, P.-C. Huang, G.-H. Lee, T. Earmme, S. L. Yau, M.-C. Chen and C. Kim, *Dyes Pigm.*, 2019, **163**, 725–733.

7 M. I. Nan, E. Lakatos, G.-I. Giurgi, L. Szolga, R. Po, A. Terec, S. Jungsuttiwong, I. Grosu and J. Roncali, *Dyes Pigm.*, 2020, **181**, 108527.

8 C. Zhang and X. Zhu, *Acc. Chem. Res.*, 2017, **50**, 1342–1350.

9 S. Vegiraju, C.-Y. Lin, P. Priyanka, D.-Y. Huang, X.-L. Luo, H.-C. Tsai, S.-H. Hong, C.-J. Yeh, W.-C. Lien, C.-L. Wang, S.-H. Tung, C.-L. Liu, M.-C. Chen and A. Facchetti, *Adv. Funct. Mater.*, 2018, **28**, 1801025.

10 H. Sirringhaus, *Adv. Mater.*, 2014, **26**, 1319–1335.

11 H. Fan, H. Li, J. Han, N. McKeever, J. Yu and H. E. Katz, *ACS Sens.*, 2019, **4**, 3240–3247.

12 Y. Park, K.-J. Baeg and C. Kim, *ACS Appl. Mater. Interfaces*, 2019, **11**, 8327–8336.

13 S. T. Keene, T. P. A. van der Pol, D. Zakhidov, C. H. L. Weijtens, R. A. J. Janssen, A. Salleo and Y. van de Burgt, *Adv. Mater.*, 2020, **32**, 2000270.

14 A. Luzio, F. Nübling, J. Martin, D. Fazzi, P. Selter, E. Gann, C. R. McNeill, M. Brinkmann, M. R. Hansen, N. Stingelin, M. Sommer and M. Caironi, *Nat. Commun.*, 2019, **10**, 3365.

15 Q. Liu, H. Sun, C. Blaikie, C. Caporale, S. Manzhos, K. Feron, J. M. MacLeod, M. Massi, S. E. Bottle, J. Bell, Y.-Y. Noh and P. Sonar, *New J. Chem.*, 2018, **42**, 12374–12385.

16 Y. Wang, H. Guo, A. Harbuzaru, M. A. Uddin, I. Arrechea-Marcos, S. Ling, J. Yu, Y. Tang, H. Sun, J. T. López Navarrete, R. P. Ortiz, H. Y. Woo and X. Guo, *J. Am. Chem. Soc.*, 2018, **140**, 6095–6108.

17 J. T. E. Quinn, J. Zhu, X. Li, J. Wang and Y. Li, *J. Mater. Chem. C*, 2017, **5**, 8654–8681.

18 L. Ren, D. Yuan and X. Zhu, *Chem. – Asian J.*, 2019, **14**, 1717–1722.

19 C.-a. Di, F. Zhang and D. Zhu, *Adv. Mater.*, 2013, **25**, 313–330.

20 Y. Shibuya, K. Aonuma, T. Kimura, T. Kaneko, W. Fujiwara, Y. Yamaguchi, D. Kumaki, S. Tokito and H. Katagiri, The, *J. Phys. Chem. C*, 2020, **124**, 4738–4746.

21 Y. Teshima, M. Saito, T. Fukuhara, T. Mikie, K. Komeyama, H. Yoshida, H. Ohkita and I. Osaka, *ACS Appl. Mater. Interfaces*, 2019, **11**, 23410–23416.

22 H. Usta, D. Kim, R. Ozdemir, Y. Zorlu, S. Kim, M. C. Ruiz Delgado, A. Harbuzaru, S. Kim, G. Demirel, J. Hong, Y.-G. Ha, K. Cho, A. Facchetti and M.-G. Kim, *Chem. Mater.*, 2019, **31**, 5254–5263.

23 M.-H. Yoon, C. Kim, A. Facchetti and T. J. Marks, *J. Am. Chem. Soc.*, 2006, **128**, 12851–12869.

24 J. A. Letizia, A. Facchetti, C. L. Stern, M. A. Ratner and T. J. Marks, *J. Am. Chem. Soc.*, 2005, **127**, 13476–13477.

25 M.-H. Yoon, S. A. DiBenedetto, A. Facchetti and T. J. Marks, *J. Am. Chem. Soc.*, 2005, **127**, 1348–1349.

26 J. Youn, S. Kewalramani, J. D. Emery, Y. Shi, S. Zhang, H.-C. Chang, Y.-J. Liang, C.-M. Yeh, C.-Y. Feng, H. Huang, C. Stern, L.-H. Chen, J.-C. Ho, M.-C. Chen, M. J. Bedzyk, A. Facchetti and T. J. Marks, *Adv. Funct. Mater.*, 2013, **23**, 3850–3865.

27 M.-C. Chen, C. Kim, S.-Y. Chen, Y.-J. Chiang, M.-C. Chung, A. Facchetti and T. J. Marks, *J. Mater. Chem.*, 2008, **18**, 1029–1036.

28 H. Reiss, L. Ji, J. Han, S. Koser, O. Tverskoy, J. Freudenberg, F. Hinkel, M. Moos, A. Friedrich, I. Krummenacher, C. Lambert, H. Braunschweig, A. Dreuw, T. B. Marder and U. H. F. Bunz, *Angew. Chem., Int. Ed.*, 2018, **57**, 9543–9547.

29 M. Chu, J.-X. Fan, S. Yang, D. Liu, C. F. Ng, H. Dong, A.-M. Ren and Q. Miao, *Adv. Mater.*, 2018, **30**, 1803467.

30 C. Wang, Z. Liang, Y. Liu, X. Wang, N. Zhao, Q. Miao, W. Hu and J. Xu, *J. Mater. Chem.*, 2011, **21**, 15201–15204.

31 Y. Qiao, Y. Guo, C. Yu, F. Zhang, W. Xu, Y. Liu and D. Zhu, *J. Am. Chem. Soc.*, 2012, **134**, 4084–4087.

32 N. Zhou, S. Vegiraju, X. Yu, E. F. Manley, M. R. Butler, M. J. Leonardi, P. Guo, W. Zhao, Y. Hu, K. Prabakaran, R. P. H. Chang, M. A. Ratner, L. X. Chen, A. Facchetti, M.-C. Chen and T. J. Marks, *J. Mater. Chem. C*, 2015, **3**, 8932–8941.

33 Y.-J. Hwang, N. M. Murari and S. A. Jenekhe, *Polym. Chem.*, 2013, **4**, 3187–3195.

34 M. J. Sung, A. Luzio, W.-T. Park, R. Kim, E. Gann, F. Maddalena, G. Pace, Y. Xu, D. Natali, C. de Falco, L. Dang, C. R. McNeill, M. Caironi, Y.-Y. Noh and Y.-H. Kim, *Adv. Funct. Mater.*, 2016, **26**, 4984–4997.

35 A. Welford, S. Maniam, E. Gann, X. Jiao, L. Thomsen, S. J. Langford and C. R. McNeill, *Org. Electron.*, 2019, **75**, 105378.

36 K. Zhou, H. Dong, H.-L. Zhang and W. Hu, *Phys. Chem. Chem. Phys.*, 2014, **16**, 22448–22457.

37 M.-C. Chen, Y.-J. Jiang, C. Kim, Y.-J. Guo, S.-Y. Chen, Y.-J. Liang, Y.-W. Huang, T.-S. Hu, G.-H. Lee, A. Facchetti and T. J. Marks, *Chem. Commun.*, 2009, 1846–1848.

38 J. Youn, P.-Y. Huang, Y.-W. Huang, M.-C. Chen, Y.-J. Lin, H. Huang, R. P. Ortiz, C. Stern, M.-C. Chung, C.-Y. Feng, L.-H. Chen, A. Facchetti and T. J. Marks, *Adv. Funct. Mater.*, 2012, **22**, 48–60.

39 J. Youn, S. Vegiraju, J. D. Emery, B. J. Leever, S. Kewalramani, S. J. Lou, S. Zhang, K. Prabakaran, Y. Ezhumalai, C. Kim,

This journal is © The Royal Society of Chemistry 2020

J. Mater. Chem. C, 2020, **8**, 15450–15458 | **15457**

P.-Y. Huang, C. Stern, W.-C. Chang, M. J. Bedzyk, L. X. Chen, M.-C. Chen, A. Facchetti and T. J. Marks, *Adv. Electron. Mater.*, 2015, **1**, 1500098.

40 Y. Didane, P. Marsal, F. Fages, A. Kumagai, N. Yoshimoto, H. Brisset and C. Videlot-Ackermann, *Thin Solid Films*, 2010, **519**, 578–586.

41 C. Zhang, Y. Zang, E. Gann, C. R. McNeill, X. Zhu, C.-A. Di and D. Zhu, *J. Am. Chem. Soc.*, 2014, **136**, 16176–16184.

42 K. Kawabata, M. Saito, I. Osaka and K. Takimiya, *J. Am. Chem. Soc.*, 2016, **138**, 7725–7732.

43 S. Vegiraju, A. A. Amelenan Torimtubun, P.-S. Lin, H.-C. Tsai, W.-C. Lien, C.-S. Chen, G.-Y. He, C.-Y. Lin, D. Zheng, Y.-F. Huang, Y.-C. Wu, S.-L. Yau, G.-H. Lee, S.-H. Tung, C.-L. Wang, C.-L. Liu, M.-C. Chen and A. Facchetti, *ACS Appl. Mater. Interfaces*, 2020, **12**, 25081–25091.

44 C. Zhang, S. Medina Rivero, W. Liu, D. Casanova, X. Zhu and J. Casado, *Angew. Chem., Int. Ed.*, 2019, **58**, 11291–11295.

45 J. Casado, R. Ponce Ortiz and J. T. López Navarrete, *Chem. Soc. Rev.*, 2012, **41**, 5672–5686.

46 K. Yang, X. Zhang, A. Harbuzaru, L. Wang, Y. Wang, C. Koh, H. Guo, Y. Shi, J. Chen, H. Sun, K. Feng, M. C. Ruiz Delgado, H. Y. Woo, R. P. Ortiz and X. Guo, *J. Am. Chem. Soc.*, 2020, **142**, 4329–4340.

47 T. Lei, J.-Y. Wang and J. Pei, *Chem. Mater.*, 2014, **26**, 594–603.

48 J. Mei and Z. Bao, *Chem. Mater.*, 2014, **26**, 604–615.

49 F. Zhang, Y. Hu, T. Schuettfort, C.-A. Di, X. Gao, C. R. McNeill, L. Thomsen, S. C. B. Mannsfeld, W. Yuan, H. Sirringhaus and D. Zhu, *J. Am. Chem. Soc.*, 2013, **135**, 2338–2349.

50 H. Huang, Z. Chen, R. P. Ortiz, C. Newman, H. Usta, S. Lou, J. Youn, Y.-Y. Noh, K.-J. Baeg, L. X. Chen, A. Facchetti and T. Marks, *J. Am. Chem. Soc.*, 2012, **134**, 10966–10973.

51 S. Vegiraju, B.-C. Chang, P. Priyanka, D.-Y. Huang, K.-Y. Wu, L.-H. Li, W.-C. Chang, Y.-Y. Lai, S.-H. Hong, B.-C. Yu, C.-L. Wang, W.-J. Chang, C.-L. Liu, M.-C. Chen and A. Facchetti, *Adv. Mater.*, 2017, **29**, 1702414.

52 H. Huang, L. Yang, A. Facchetti and T. J. Marks, *Chem. Rev.*, 2017, **117**, 10291–10318.

53 S. Vegiraju, X.-L. Luo, L.-H. Li, S. N. Afraj, C. Lee, D. Zheng, H.-C. Hsieh, C.-C. Lin, S.-H. Hong, H.-C. Tsai, G.-H. Lee, S.-H. Tung, C.-L. Liu, M.-C. Chen and A. Facchetti, *Chem. Mater.*, 2020, **32**, 1422–1429.

54 Y. Ezhumalai, F.-S. Lin, M.-S. Fan, K. Prabakaran, J.-S. Ni, Y.-C. Wu, G.-H. Lee, M.-C. Chen and K.-C. Ho, *ACS Appl. Mater. Interfaces*, 2020, **12**, 15071–15079.

55 Y. Qiao, J. Zhang, W. Xu and D. Zhu, *J. Mater. Chem.*, 2012, **22**, 5706–5714.

56 H. Jiang, K. Oniwa, Z. Xu, M. Bao, Y. Yamamoto and T. Jin, *Bull. Chem. Soc. Jpn.*, 2017, **90**, 789–797.

57 C. Zhang and X. Zhu, *Adv. Funct. Mater.*, 2020, **30**, 2000765.

58 Y. Kunugi, K. Takimiya, Y. Toyoshima, K. Yamashita, Y. Aso and T. Otsubo, *J. Mater. Chem.*, 2004, **14**, 1367–1369.

59 R. J. Chesterfield, C. R. Newman, T. M. Pappenfus, P. C. Ewbank, M. H. Haukaas, K. R. Mann, L. L. Miller and C. D. Frisbie, *Adv. Mater.*, 2003, **15**, 1278–1282.

60 T. M. Pappenfus, R. J. Chesterfield, C. D. Frisbie, K. R. Mann, J. Casado, J. D. Raff and L. L. Miller, *J. Am. Chem. Soc.*, 2002, **124**, 4184–4185.

61 D. E. Janzen, M. W. Burand, P. C. Ewbank, T. M. Pappenfus, H. Higuchi, D. A. da Silva Filho, V. G. Young, J.-L. Bredas and K. R. Mann, *J. Am. Chem. Soc.*, 2004, **126**, 15295–15308.

62 S. Handa, E. Miyazaki, K. Takimiya and Y. Kunugi, *J. Am. Chem. Soc.*, 2007, **129**, 11684–11685.

63 Q. Wu, R. Li, W. Hong, H. Li, X. Gao and D. Zhu, *Chem. Mater.*, 2011, **23**, 3138–3140.

64 Y. Kim, H. Hwang, N.-K. Kim, K. Hwang, J.-J. Park, G.-I. Shin and D.-Y. Kim, *Adv. Mater.*, 2018, **30**, 1706557.

65 Y. Suzuki, M. Shimawaki, E. Miyazaki, I. Osaka and K. Takimiya, *Chem. Mater.*, 2011, **23**, 795–804.

66 N. Elfers, I. Lyskov, J. D. Spiegel and C. M. Marian, *J. Phys. Chem. C*, 2016, **120**, 13901–13910.

67 M. V. Ivanov, D. Wang, S. H. Wadumethridge and R. Rathore, *J. Phys. Chem. Lett.*, 2017, **8**, 4226–4230.

68 J. C. Ribierre, L. Zhao, S. Furukawa, T. Kikitsu, D. Inoue, A. Muranaka, K. Takaishi, T. Muto, S. Matsumoto, D. Hashizume, M. Uchiyama, P. André, C. Adachi and T. Aoyama, *Chem. Commun.*, 2015, **51**, 5836–5839.

69 K. Guo, B. Wu, Y. Jiang, Z. Wang, Z. Liang, Y. Li, Y. Deng and Y. Geng, *J. Mater. Chem. C*, 2019, **7**, 10352–10359.

70 R. Pfattner, C. Rovira and M. Mas-Torrent, *Phys. Chem. Chem. Phys.*, 2015, **17**, 26545–26552.

71 R. Schroeder, L. A. Majewski and M. Grell, *Appl. Phys. Lett.*, 2003, **83**, 3201.

72 H. Bronstein, C. B. Nielsen, B. C. Schroeder and I. McCulloch, *Nat. Rev. Chem.*, 2020, **4**, 66–77.

73 D. M. de Leeuw, M. M. J. Simenon, A. R. Brown and R. E. F. Einerhand, *Synth. Met.*, 1997, **87**, 53–59.

74 S. Park, S. H. Kim, H. H. Choi, B. Kang and K. Cho, *Adv. Funct. Mater.*, 2020, **30**, 1904590.

15458 | *J. Mater. Chem. C*, 2020, **8**, 15450–15458

This journal is © The Royal Society of Chemistry 2020